

The Impact of Positive-Definite Moisture Transport on NWP Precipitation Forecasts

WILLIAM C. SKAMAROCK AND MORRIS L. WEISMAN

National Center for Atmospheric Research, Boulder, Colorado*

(Manuscript received 4 March 2008, in final form 7 July 2008)

ABSTRACT

A positive-definite transport scheme for moisture is tested in a nonhydrostatic forecast model using convection-permitting resolutions. Use of the positive-definite scheme is found to significantly reduce the large positive bias in surface precipitation forecasts found in the non-positive-definite model forecasts, in particular at high precipitation thresholds. The positive-definite scheme eliminates spurious sources of water arising from the clipping of negative moisture values in the non-positive-definite model formulation, leading to the bias reduction.

1. Introduction

With the growing use of nonhydrostatic NWP models configured to explicitly represent deep convective clouds and precipitation, the numerical transport schemes used in these models must handle increasingly strong gradients and discontinuities present in the simulated cloud and precipitation fields. Although recent real-time convective forecasting experiments, using horizontal grid spacings of 2–4 km, show promise in offering enhanced guidance for forecasting convective system mode and evolution, these forecasts have exhibited a systematic positive bias in precipitation amounts, especially for the higher precipitation thresholds often associated with deep convection (e.g., Done et al. 2004; Weisman et al. 2008; Kain et al. 2008). While several factors may be contributing to this bias, including using resolutions that are still marginal for fully representing convective processes (e.g., Bryan et al. 2003), the formulation and performance of the moisture transport schemes can also be a significant contributor. The effect of moisture transport schemes on precipitation is the explicit emphasis of the present work.

The fully conservative formulations used in the latest generation of nonhydrostatic NWP models [e.g., the Advanced Research version of the Weather Research and Forecasting Model (ARW); Skamarock and Klemp 2008; Skamarock et al. 2005] allow the computation of exact water budgets (to machine round off). We have been examining these water budgets, using both idealized simulations of convection and NWP test cases, and have compared the results from the ARW simulations with and without positive-definite (PD) transport of moisture. We have found that there is a significant spurious source of water when PD schemes are not used for moisture transport in the ARW test simulations. These spurious sources arise from the clipping of negative water species mixing ratios produced by the standard (non PD) ARW advection scheme. The term clipping refers to setting any negative mixing ratios to zero after the transport step is complete. This spurious water source is significant relative to many important water-budget quantities, with perhaps the most important consequence being the significant increase in precipitation resulting from the use of the non-PD scheme.

In some models that have nonconservative formulations, these clipping problems have been addressed by using PD scheme techniques (e.g., Wicker and Wilhelmson 1995; Xue et al. 2000), although PD results are no longer guaranteed. In other nonconservative models the clipping problem has not been addressed nor evaluated. In this note we present the formulation of the non-PD and PD transport schemes used in the ARW model, together with results demonstrating the benefi-

* The National Center for Atmospheric Research is sponsored by the National Science Foundation.

Corresponding author address: William C. Skamarock, National Center for Atmospheric Research, P.O. Box 3000, Boulder, CO 80307-3000.
E-mail: skamaroc@ucar.edu

cial impact of the PD scheme on the moisture budget and precipitation forecasts.

2. ARW positive-definite transport formulation

The scalar conservation equation integrated in the ARW model can be written as

$$\frac{\partial \mu \phi}{\partial t} + \frac{\partial \mu \mu \phi}{\partial x} + \frac{\partial \mu \nu \phi}{\partial y} + \frac{\partial \mu \dot{\eta} \phi}{\partial \eta} = \mu S_\phi, \quad (1)$$

where ϕ is the scalar mixing ratio, μ is the column mass (in the mass, or hydrostatic pressure, vertical coordinate), η is the vertical coordinate, and the other variables have their usual meaning. The ARW model uses a third-order Runge–Kutta method to integrate (1), and this discrete integration can be expressed as

$$(\mu \phi)^* = (\mu \phi)^t - \frac{\Delta t}{3} \left(\sum_i \delta_{x_i} F_{x_i}^t - \mu S_\phi^t \right), \quad (2a)$$

$$(\mu \phi)^{**} = (\mu \phi)^t - \frac{\Delta t}{2} \left(\sum_i \delta_{x_i} F_{x_i}^{**} - \mu S_\phi^t \right), \quad (2b)$$

and

$$(\mu \phi)^{t+\Delta t} = (\mu \phi)^t - \Delta t \left(\sum_i \delta_{x_i} F_{x_i}^{**} - \mu S_\phi^t \right), \quad (2c)$$

where the superscripts denote the time level; the asterisk and double-asterisk superscripts denote the $t + \Delta t/3$ and $t + \Delta t/2$ predictors, respectively, in the Runge–Kutta integration; and $\delta_{x_i} F_{x_i}$ denotes the centered flux divergence operator in the i th coordinate direction. For example, in the x direction:

$$\delta_x F_x = \Delta x^{-1} [F(\mu, u, \phi; x + \Delta x/2) - F(\mu, u, \phi; x - \Delta x/2)].$$

The default flux operators for ARW are fifth-order operators for the horizontal flux calculations and a third-order operator for the vertical flux calculation (see Skamarock et al. 2005).

The integration scheme (2) using the standard flux operators is not positive definite nor monotonic, and it can generate negative mixing ratios even though it conserves exactly. A positive-definite transport scheme has been introduced into the ARW model that is based on the integration scheme (2) and the flux renormalization described in Skamarock (2006). The PD transport scheme replaces the final Runge–Kutta step (2c) with

$$(\mu \phi)^{***} = (\mu \phi)^t + \Delta t \mu S_\phi^t \quad \text{and} \quad (3a)$$

$$(\mu \phi)^{t+\Delta t} = (\mu \phi)^{***} - \Delta t \sum_i \delta_{x_i} [F_{x_i}^{1***} + R(F_{x_i}^{\text{cor**}})], \quad (3b)$$

where $R(F)$ denotes a renormalized flux and F^1 denotes a first-order upwind flux. In (3) we compute the upwind flux F^{1***} using ϕ^{***} , that is, using ϕ^t updated with the source terms (in the ARW these are the physics tendencies and explicit mixing terms). The full fluxes $F_{x_i}^{***}$ are calculated along with the first-order upwind fluxes (denoted $F_{x_i}^{1***}$), and the full flux is partitioned between a first-order flux (the upwind flux) and a high-order correction:

$$F_{x_i}^{\text{cor**}} = F_{x_i}^{***} - F_{x_i}^{1***}.$$

The scalar mass $\mu \phi^{***}$ is then updated using the first-order upwind fluxes:

$$(\widetilde{\mu \phi}) = (\mu \phi)^{***} - \Delta t \sum_i \delta_{x_i} F_{x_i}^{1***}. \quad (4)$$

The physics update (3a) is positive definite, and the update (4), using fluxes computed in the update (3a), is monotonic and positive definite. Next, we determine if addition of the outgoing higher-order correction fluxes will result in negative mixing ratios (only outgoing fluxes decrease the mixing ratio in a cell):

$$(\mu \phi)^{t+\Delta t} < 0 \quad \text{if } (\widetilde{\mu \phi}) < \Delta t \sum_i \delta_{x_i} (F_{x_i}^{\text{cor**}})^+. \quad (5)$$

If a negative mixing ratio is indicated, these outgoing fluxes $(F_{x_i}^{\text{cor**}})^+$ are renormalized:

$$R(F_{x_i}^{\text{cor**}})^+ = (F_{x_i}^{\text{cor**}})^+ \widetilde{\mu \phi} \left[\Delta t \sum_i \delta_{x_i} (F_{x_i}^{\text{cor**}})^+ \right]^{-1}, \quad (6a)$$

and the flux is retained if no negative mixing ratio is indicated by (5):

$$R(F_{x_i}^{\text{cor**}})^+ = (F_{x_i}^{\text{cor**}})^+. \quad (6b)$$

The renormalized higher-order correction fluxes are used in a final update, completing the update (3b). The renormalization (6) prevents the outgoing fluxes from driving the scalar mass below zero [the outgoing fluxes are renormalized in (6a) such that their addition will drive the scalar mass exactly to zero].

Our renormalization scheme is very similar to the monotonic multidimensional flux-corrected transport scheme introduced by Zalesak (1979). The primary differences between the algorithms are the underlying high-order transport schemes (a multistep Runge–Kutta scheme with third- and fifth-order spatial approximations used here as opposed to the several different schemes tested in Zalesak) and the use of a positive-definite renormalization that is a special case of the monotonic renormalization used by Zalesak.

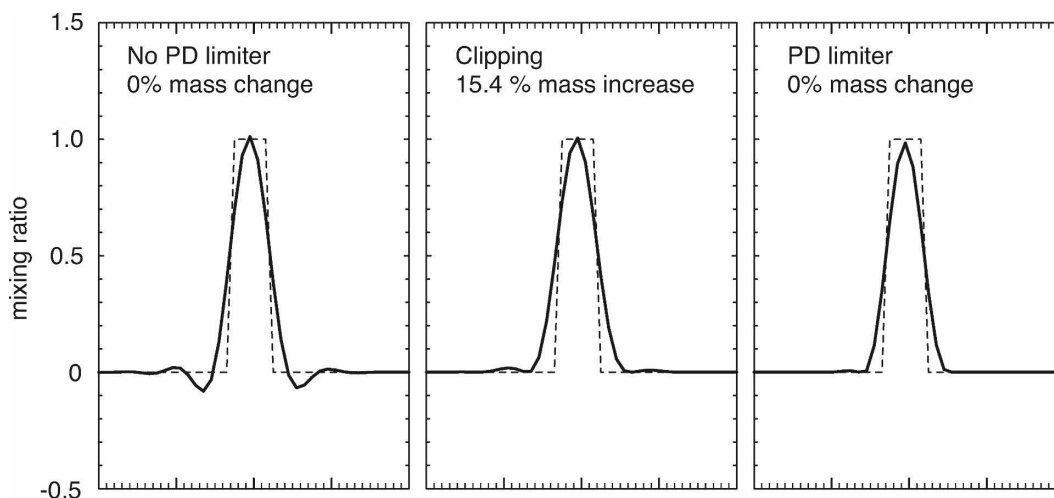


FIG. 1. The 1D advection of a square wave in a periodic domain of length $100\Delta x$. The initial square wave is plotted with a dashed line, and its width is $5\Delta x$. The solution after a single revolution using 200 time steps and a fixed Courant number of 0.5 is plotted as a solid line. Only the middle 40% of the domain is plotted.

When renormalization occurs, the stability of the transport scheme should approach that of the multidimensional first-order upwind scheme. The stability constraint for the multidimensional first-order upwind scheme is significantly less than that of the multidimensional Runge–Kutta-based scheme. In practice, however, we have not encountered any model instabilities or solution abnormalities associated with the renormalization scheme. It appears that the potential linear instabilities are not encountered in practice because the average Courant numbers of the transport are usually small (large Courant numbers are limited to very small regions in the solution) and because the renormalization is typically active only on a small number of cell faces.

To illustrate the effects of clipping and of the renormalization scheme by way of a simple example, Fig. 1 shows the results from three simulations of a 1D square wave transported over a single revolution in a periodic domain. There are 100 points in the domain, the Courant number $U\Delta t/\Delta x = 0.5$, and the 1D version of the transport equation [i.e., (1)] is integrated using the Runge–Kutta scheme (2) with the fifth-order transport operator for 200 time steps. The square wave has an initial width of $5\Delta x$, that is, the width of a poorly resolved feature in an NWP model such as a convective cloud using a grid spacing of order 1 km. The non-PD solution is plotted on the left; it shows significant negative values of the tracer mixing ratio in addition to significant distortion of the poorly resolved square wave. Tracer mass is conserved exactly in this integration because the negative mass is offset by an increase in positive mass. The middle panel in Fig. 1 depicts the solu-

tion computed with negative values clipped after each time step. This clipping is the same as that occurring to negative moisture values in ARW simulations where the PD scheme is not used. The clipping removes the negative moisture values but results in an approximately 15.4% increase in the integrated tracer mass. Mass is no longer conserved when clipping negative mixing ratios—it is increased by the amount of clipped tracer mass. The right panel in Fig. 1 shows the PD solution computed using the flux renormalization (3)–(6). The negative values of the tracer are completely removed and tracer mass is conserved. There is also an indication that there is slightly less numerical dispersion relative to the solution using clipping.

3. Forecast examples

We have been using the ARW model to produce real-time forecasts for the 2003–07 spring–summer convective seasons over the central United States, and the model was configured with a horizontal grid spacing of 4 km in 2003–06 and a horizontal grid spacing of 3 km in 2007. Forecasts were initialized at 0000 UTC and extended through 36 h. The PD moisture transport was used in the 2007 forecasts, and the non-PD scheme was used in years previous to 2007 [the PD option for ARW made available to the community in the December 2006 version-2.2 Weather Research and Forecasting Model (WRF) release]. We begin by presenting individual case studies from 2005 and 2007, to document the generic impacts of including the PD transports, and then compare the biases for the PD versus non-PD forecasts for the full 2005 versus 2007 seasons. Because grid reso-

lution and other aspects of the model formulation also changed between these years [e.g., the Yonsei University PBL scheme and the WRF Single-Moment 6-Class (WSM6) microphysics scheme was applied in 2005, whereas the Mellor–Yamada–Janjic PBL scheme and the Thompson microphysics scheme was applied in 2007, along with other minor bug fixes and changes in initialization], the comparison between the seasons is largely qualitative.

a. Case studies—5 June 2005 and 14 April 2007

The two cases chosen are representative of heavy precipitation, severe convective outbreaks in the high plains, and were both forecast reasonably well by the ARW. On 5 June 2005, a severe squall line with embedded supercells developed along a dryline near, from Nebraska southward through Oklahoma around 0000 UTC (24 h into the forecast period), in response to a moderately strong synoptic-scale wave moving eastward from the Rockies. This case is also discussed in Weisman et al. (2008), where it is shown that the forecast was relatively insensitive to variations in model physics and initialization procedures. On 14 April 2007, a strong synoptic-scale cyclone moved eastward across Texas, Oklahoma, Kansas, Missouri, and Arkansas, with widespread, heavy stratiform precipitation and embedded convection occurring over most of this region. A severe squall line with embedded supercells was also observed in the warm sector over central and eastern Texas.

Figure 2 shows the 24-h accumulated precipitation valid at 1200 UTC 5 June 2005 and 14 April 2007, from the stage-4 precipitation analysis, the 12–36-h ARW forecasts using the standard (non PD) moisture transport scheme, and the ARW forecasts using the PD moisture transport scheme. The forecasts using different transport schemes contain some significant errors evaluated against the stage-4 analysis for both cases. The ARW PD and non-PD forecasts are similar in many respects, but the PD-based forecast show a significant reduction in the areas of higher precipitation amounts relative to the non-PD forecast. This subjective evaluation also suggests that the overall area of measurable precipitation is somewhat reduced in the PD forecasts.

Figure 3 depicts the bias for the 24-h accumulated precipitation PD and non-PD ARW forecasts for the 5 June 2005 and 14 April 2007 cases, respectively. The most significant result is that the positive biases have been reduced by approximately a factor of 2 across all precipitation thresholds, and by significantly more than this at high precipitation thresholds for the 14 April 2007 case. Perhaps most important, the strong positive

biases at high thresholds have been substantially reduced. Most of the precipitation is accumulated at these higher thresholds as indicated by the percentage accumulation plotted in the figure for both cases.

The net precipitation amounts in the PD and non-PD forecasts for these two cases, along with the water added by clipping in the non-PD forecasts, are given in Table 1. The non-PD ARW forecasts produced approximately 21% and 35% more surface precipitation than the PD ARW forecasts for 5 June 2005 and 14 April 2007 cases, respectively. For the 5 June 2005 case, the increase in surface precipitation (9×10^{12} kg) is approximately 2/3 of the amount of water added spuriously by clipping (14.3×10^{12} kg). For the 14 April 2007 case, the increase in surface precipitation (13.8×10^{12} kg) is approximately 90% of the amount of water added spuriously by clipping (15.4×10^{12} kg). We have not attempted to directly trace the precipitation that arose from water added spuriously by clipping, but we have instrumented the ARW model to track the mass of clipped water added to different moist species, and these results appear in Table 1. No additional moisture appears in the vapor field, likely because it has a non-zero background value and clipping is never necessary. Most of the additional moisture appears as cloud, followed by rain and graupel and snow. To appear as surface precipitation in the ARW forecasts, cloud water must be converted to a precipitating species (rain, snow, or graupel) and then fall to the surface. Thus, much of the additional surface precipitation is not a direct result of increasing the precipitating species, but rather by increasing their precursor—cloud water.

b. 2005 and 2007 forecast seasons

Statistics for the full 2005 and 2007 forecast seasons are presented in Fig. 4. Again, the ARW model did not use PD advection in real time during the 2005 forecast season, while PD advection was used in the 2007 forecast season. As shown for the above individual case studies, without PD advection, the bias for the 2005 forecast season shows a dramatically increasing positive bias for thresholds greater than approximately half an inch. The bias in the 2007 season also increases with increasing threshold, but at a much smaller and relatively constant rate in comparison with the 2005 season bias. Also shown in Fig. 4 is the percentage of the total precipitation as a function of the threshold, computed from the 2007 stage-4 analyses. Fifty percent of the precipitation is associated with 24-h precipitation thresholds somewhat greater than 0.5 in. (~ 1.3 cm). This region is where the strong and growing positive bias of the non-PD forecasts is most pronounced.

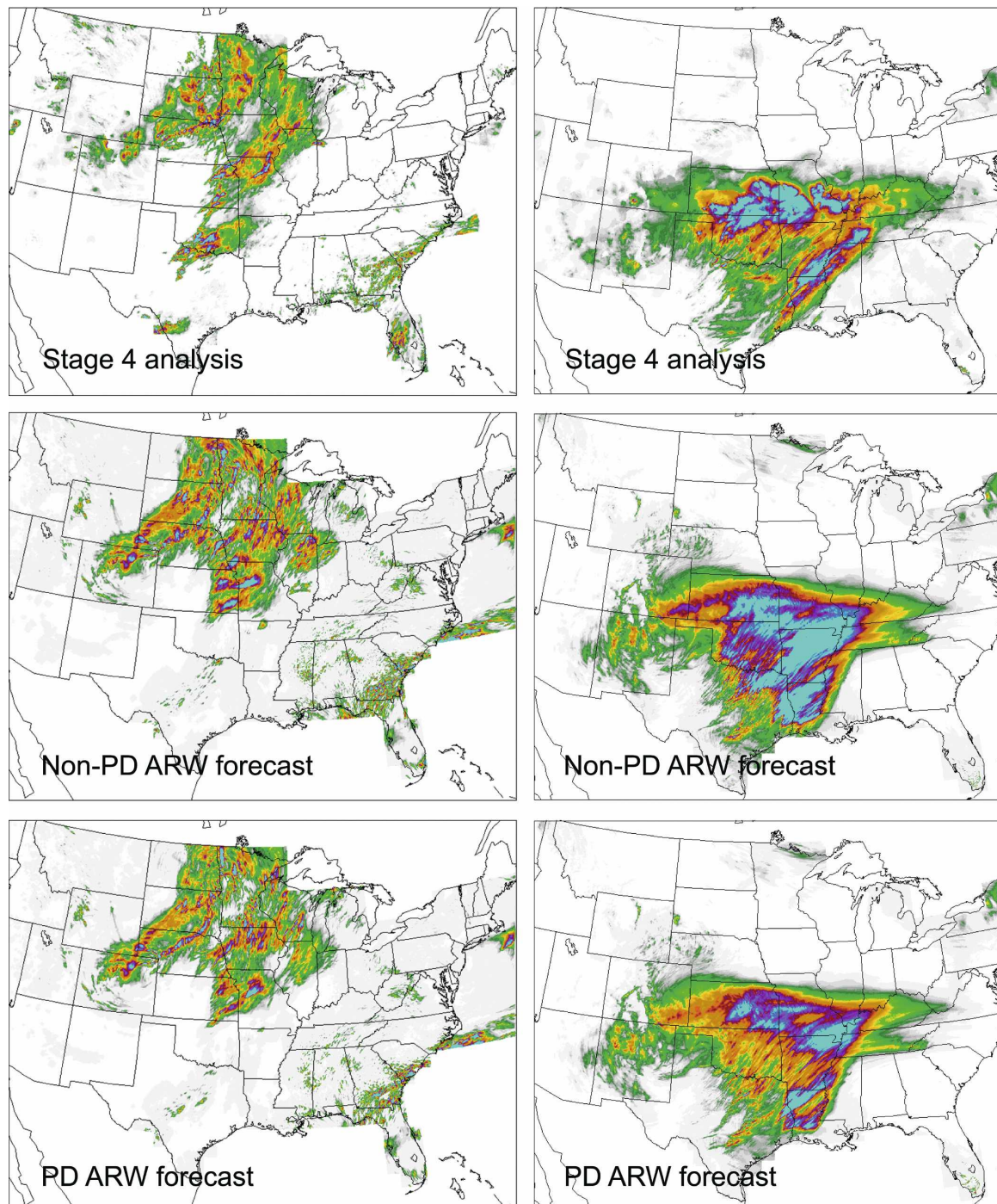


FIG. 2. The 24-h accumulated precipitation valid at (left) 1200 UTC 5 Jun 2005 and (right) 1200 UTC 14 Apr 2007: (top) stage-4 analyses, (middle) 12–36-h ARW non-PD forecasts, and (bottom) 12–36-h ARW PD forecasts.

4. Discussion

It is difficult to numerically forecast high-precipitation events accurately in a deterministic manner because these events are most often small scale in both space and time. It is, however, important

that the frequency and spatial scales of these events be accurately predicted by the model forecasts so that probabilistic forecasts can be attempted, either subjectively by forecasters examining individual forecasts, or objectively using ensemble forecasting techniques.

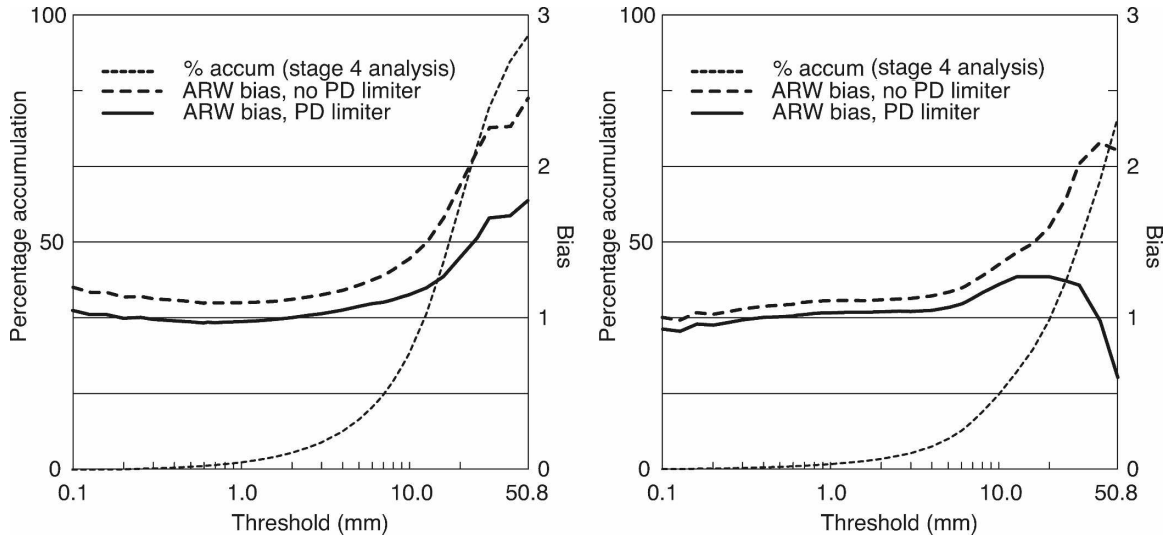


FIG. 3. The 24-h accumulated precipitation biases for the PD and non-PD ARW forecasts valid at (left) 1200 UTC 5 Jun 2005 and (right) 1200 UTC 14 Apr 2007. The percentage accumulation for the stage-4 analyses are also plotted.

The use of the PD limiter in the ARW model has remedied an obvious physical error in the forecasts—the nonconservation of water. We have demonstrated that the PD limiter has a major positive benefit on the precipitation forecast bias. The use of the PD scheme has not completely removed the positive bias observed in the high-resolution forecasts. Other aspects of the ARW formulation that may be responsible for the remaining bias are the mixing parameterizations and the representation of explicit and subgrid clouds and precipitation processes. Other objective measures of the forecast skill, such as equitable threat scores, are not significantly affected by the PD limiter. The impact of the PD limiter on precipitation is significantly reduced as the horizontal grids become coarser to the point where a convective parameterization becomes respon-

sible for the majority of the surface precipitation; thus, our results are primarily relevant for convection-permitting resolutions where clouds and convective elements are poorly resolved.

Other models may benefit from using positive-definite transport algorithms, although the results reported here are not necessarily directly applicable. Other nonhydrostatic modeling systems using split-explicit time integration techniques similar to that used in ARW [e.g., the Advanced Regional Prediction Sys-

TABLE 1. Precipitation and spurious water added through clipping in the non-PD forecasts for the 5 Jun 2005 and 14 Apr 2007 cases. The precipitation totals and water budgets are for the 24-h period ending at 1200 UTC.

Water species (10^{12} kg)	5 Jun 2005	14 Apr 2007
Tot precipitation, PD	43.47	39.20
Tot precipitation, non-PD	52.55	52.96
Non-PD added water		
Vapor	0.00	0.00
Cloud	9.36	11.30
Rain	2.32	2.03
Ice	0.47	0.06
Snow	0.33	1.08
Graupel	1.86	0.91
Tot added water	14.34	15.38

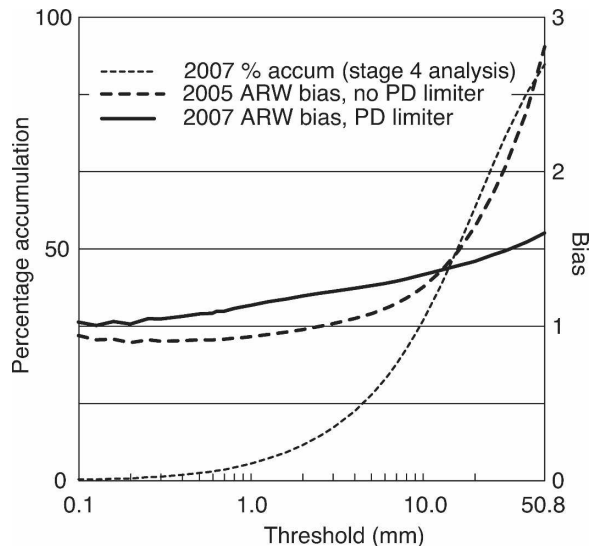


FIG. 4. The 24-h accumulated precipitation biases for the PD and non-PD ARW forecasts valid for the 2005 and 2007 forecast seasons.

tem (Xue et al. 2000), the Coupled Ocean–Atmosphere Mesoscale Prediction System (Hodur 1997), the Regional Atmospheric Modeling System (Pielke et al. 1992), and the Lokal Modell (Doms and Schättler 2002)] are not formulated in conservative form; hence, the flux limiting outlined in this paper could not be directly applied, but they can be used to some effect by recasting the transport equation and using the flux-form algorithms. In Wicker and Wilhelmson (1995) and Xue et al. (2000), the transport equation is written as

$$\frac{D\phi}{Dt} = \frac{\partial\phi}{\partial t} + \mathbf{V} \cdot \nabla\phi = \frac{\partial\phi}{\partial t} + \frac{1}{\bar{\rho}} [\nabla \cdot (\bar{\rho}\mathbf{V}\phi) - \phi\nabla \cdot (\bar{\rho}\mathbf{V})],$$

where $\bar{\rho}(z)$ is a reference density profile. Conservative positive-definite transport schemes can be applied to the term $\nabla \cdot (\bar{\rho}\mathbf{V}\phi)$ with beneficial effects similar to those reported here (e.g., Wicker and Wilhelmson 1995; Xue et al. 2001), but the overall schemes are not conservative and the PD behavior is not guaranteed because of the existence of the $\phi\nabla \cdot (\bar{\rho}\mathbf{V})$ term. In addition, many of these models are based on leapfrog time discretization and second-order-centered spatial discretizations and typically use more dissipation for their NWP configurations than the ARW, thus their smoother (more damped) solutions likely show less of a positive precipitation bias from clipping. However, Xue et al. (2001) did find a significant reduction in surface precipitation when testing monotonic schemes in supercell storm simulations. Semi-Lagrangian formulations, for example the Met Office model (Staniforth and Wood 2008), use monotonic or PD interpolators coupled with a global correction to achieve positive definiteness and global conservation, and thus do not have a clipping problem. The National Centers for Environmental Prediction Nonhydrostatic Meso Model (NMM) uses a monotonic transport scheme within its conservative formulation (Z. Janjic 2005, personal communication); thus, it does not have a clipping problem. It does, however, show significantly higher precipitation biases than the non-PD ARW model at high resolution, likely because of the choice and configuration of the NMM filters and dissipation mechanisms (Skamarock and Dempsey 2005).

Acknowledgments. We thank Wei Wang and Kevin Manning for their assistance in producing and analyzing these forecasts and also Joseph Klemp and two anonymous reviewers for their careful reviews of this manuscript.

REFERENCES

- Bryan, G. H., J. C. Wyngaard, and J. M. Fritsch, 2003: Resolution requirements for the simulation of deep moist convection. *Mon. Wea. Rev.*, **131**, 2394–2416.
- Doms, G., and U. Schättler, 2002: A description of the nonhydrostatic regional model LM. Part 1. Dynamics and numerics. Deutscher Wetterdienst (DWD), Offenbach, Germany, 149 pp.
- Done, J., C. A. Davis, and M. L. Weisman, 2004: The next generation of NWP: Explicit forecasts of convection using the Weather Research and Forecasting (WRF) Model. *Atmos. Sci. Lett.*, **5**, 110–117.
- Hodur, R. M., 1997: The Naval Research Laboratory's Coupled Ocean–Atmosphere Mesoscale Prediction System (COAMPS). *Mon. Wea. Rev.*, **125**, 1414–1430.
- Kain, J. S., and Coauthors, 2008: Some practical considerations regarding horizontal resolution in the first generation of operational convection-allowing NWP. *Wea. Forecasting*, **23**, 931–952.
- Pielke, R. A., and Coauthors, 1992: A comprehensive meteorological modeling system: RAMS. *Meteor. Atmos. Phys.*, **49**, 69–91.
- Skamarock, W. C., 2006: Positive-definite and monotonic limiters for unrestricted-time-step transport schemes. *Mon. Wea. Rev.*, **134**, 2241–2250.
- , and D. Dempsey, 2005: High resolution winter season NWP: Preliminary evaluation of the WRF-ARW and WRF-NMM models in the DWFE forecast experiment. Preprints, *17th Conf. on Numerical Weather Prediction*, Washington, DC, Amer. Meteor. Soc., 16A.3.
- , and J. B. Klemp, 2008: A time-split nonhydrostatic atmospheric model for weather research and forecasting applications. *J. Comput. Phys.*, **227**, 3465–3485, doi:10.1016/j.jcp.2007.01.037.
- , —, J. Dudhia, D. Gill, D. Barker, W. Wang, and J. G. Powers, 2005: A description of the Advanced Research WRF Version 2. NCAR Tech. Note NCAR/TN-468+STR, 88 pp.
- Staniforth, A., and N. Wood, 2008: Aspects of the dynamical core of a nonhydrostatic, deep-atmosphere, unified weather and climate-prediction model. *J. Comput. Phys.*, **227**, 3445–3464, doi:10.1016/j.jcp.2006.11.009.
- Weisman, M. L., C. A. Davis, W. Wang, K. W. Manning, and J. B. Klemp, 2008: Experiences with 0–36-h explicit convective forecasts with the WRF-ARW Model. *Wea. Forecasting*, **23**, 407–437.
- Wicker, L. J., and R. B. Wilhelmson, 1995: Simulation and analysis of tornado development and decay within a 3-dimensional supercell thunderstorm. *J. Atmos. Sci.*, **52**, 2675–2703.
- Xue, M., K. K. Droegemeier, and V. Wong, 2000: The Advanced Regional Prediction System (ARPS)—A multiscale nonhydrostatic atmospheric simulation and prediction tool. Part I: Model dynamics and verification. *Meteor. Atmos. Phys.*, **75**, 161–193.
- , and Coauthors, 2001: The Advanced Regional Prediction System (ARPS)—A multiscale nonhydrostatic atmospheric simulation and prediction tool. Part II: Model physics and applications. *Meteor. Atmos. Phys.*, **76**, 143–165.
- Zalesak, S. T., 1979: Fully multidimensional flux-corrected transport algorithms for fluids. *J. Comput. Phys.*, **31**, 335–362.